ADVANCED MATERIALS TECHNOLOGIES
www.advmattechnol.d

Effects of Environmental Atmosphere on the Performance of Contact–Separation Mode TENG

*Kai Han, Wei Tang, Jian Chen, Jianjun Luo, Liang Xu, and Zhong Lin Wang**

With great potential applications, triboelectric nanogenerator (TENG), is widely studied from various aspects, while systematic investigations about the effects of environmental atmosphere on its performance remain to be carried out. Here, a test system based on a piston-structured TENG and one-way valve gas line is built, employing the contact–separation mode. A series of tests about short-circuit transfer charges (Q_{SC}) and open-circuit voltage (V_{OC}) are studied among three kinds of dielectric materials (PTFE, Kapton, PET), in five pure gases (N_2, O_2, CO_2, Ar, He). At a static gas flow rate of 3 L min^{-1} or static gas pressure of 6 kPa above 1 atm, multicycle statistics demonstrate that TENGs achieve the highest performance in CO_2 and the lowest in He. Meanwhile, Kapton-based TENG shows the greatest disparity in different atmosphere, followed by PET-based TENG, and PTFE-based TENG. A microscale discharge mechanism is introduced to explain all the above. Moreover, a negative linear relationship between Q_{SC} and the static gas pressure above 1 atm is found. This study is an important reference for a high-performance TENG configuration and device packaging in the future.

1. Introduction

Triboelectric nanogenerator (TENG), derived from the Maxwell's displacement current has shown powerful applications in mechanical energy converting, self-powered sensing system and blue energy, since invented in 2012.[1–6] Various aspects about TENG are studied to tap its potential, including basic materials, structures, working principle, and load circuit.[7–9] It is found that some factors do affect the performance of TENG, positively or negatively, such as dielectric constant,[10,11] relative humidity,[12,13] acting force,[14,15] resistance, and so on.[16–21]

Considering that studies about the effects of gases on the contact electrification has a long history,[22–28] environmental atmosphere will ineluctably play an important role in the performance of TENG. Taking water as an example, its existence in air usually shows negative impact on TENG as some previous reported works.[12,13] When the device was put in vacuum, ultrahigh charge density and efficient energy harvesting were achieved.[29] In addition, the gas atmosphere (Air, N_2, Ar) on liquid-metal based TENG was also found to affect the device's performance and the charge separation behavior.[30] However, detailed investigations about the effects of environmental atmosphere on TENG need to be carried out.

In this work, based on a piston-structured TENG and one-way valve gas line, a test system with controllable gas flow rate and pressure was built. Contact–separation mode was employed.[31] Then a series of basic performance tests were conducted among three kinds of TENGs (PTFE-based, Kapton-based, PET-based) in five pure gases (N_2, O_2, CO_2, Ar, He), respectively. Multicycle statistics demonstrated that TENGs performed almost the best in CO_2 and the worst in He. On account of these discoveries, a microscale discharge mechanism was introduced to make an explanation. In addition, a negative linear relationship between short-circuit transfer charge (Q_{SC}) and static gas pressure was also found.

2. Results and Discussion

A semi-closed test system (**Figure 1**a) was constructed, with a controlled flow and fewer testing noise factors. The piston structure by using the disposable syringe can supply a gas-tight reciprocating motion, and one-way valves can make sure the gas flow into one direction as much as possible with fresh high purity all along. Furthermore, double gas collecting bottles with concentrated sulfuric acid (98% H_2SO_4) were placed at the end of gas line to prevent external foreign molecules. On account of the property differences of five gases, two kinds of measurement principle flowmeter, glass rotameter with knob and digital flowmeter equipped with temperature sensor, were connected at the front and the back of the gas channel. At the same time, digital pressure gauge was used to monitor the gas pressure. The motion power was provided by linear

K. Han, Prof. W. Tang, J. Chen, Dr. J. Luo, Prof. L. Xu, Prof. Z. L. Wang
CAS Center for Excellence in Nanoscience
Beijing Key Laboratory of Micro-Nano Energy and Sensor
Beijing Institute of Nanoenergy and Nanosystems
Chinese Academy of Sciences
Beijing 100083, P. R. China
E-mail: zlwang@gatech.edu
K. Han, Prof. W. Tang, J. Chen, Dr. J. Luo, Prof. L. Xu, Prof. Z. L. Wang
School of Nanoscience and Technology
University of Chinese Academy of Sciences
Beijing 100049, P. R. China
Prof. Z. L. Wang
School of Materials Science and Engineering
Georgia Institute of Technology
Atlanta, GA 30332-0245, USA
The ORCID identification number(s) for the author(s) of this article can be found under https://doi.org/10.1002/admt.201800569.

DOI: 10.1002/admt.201800569

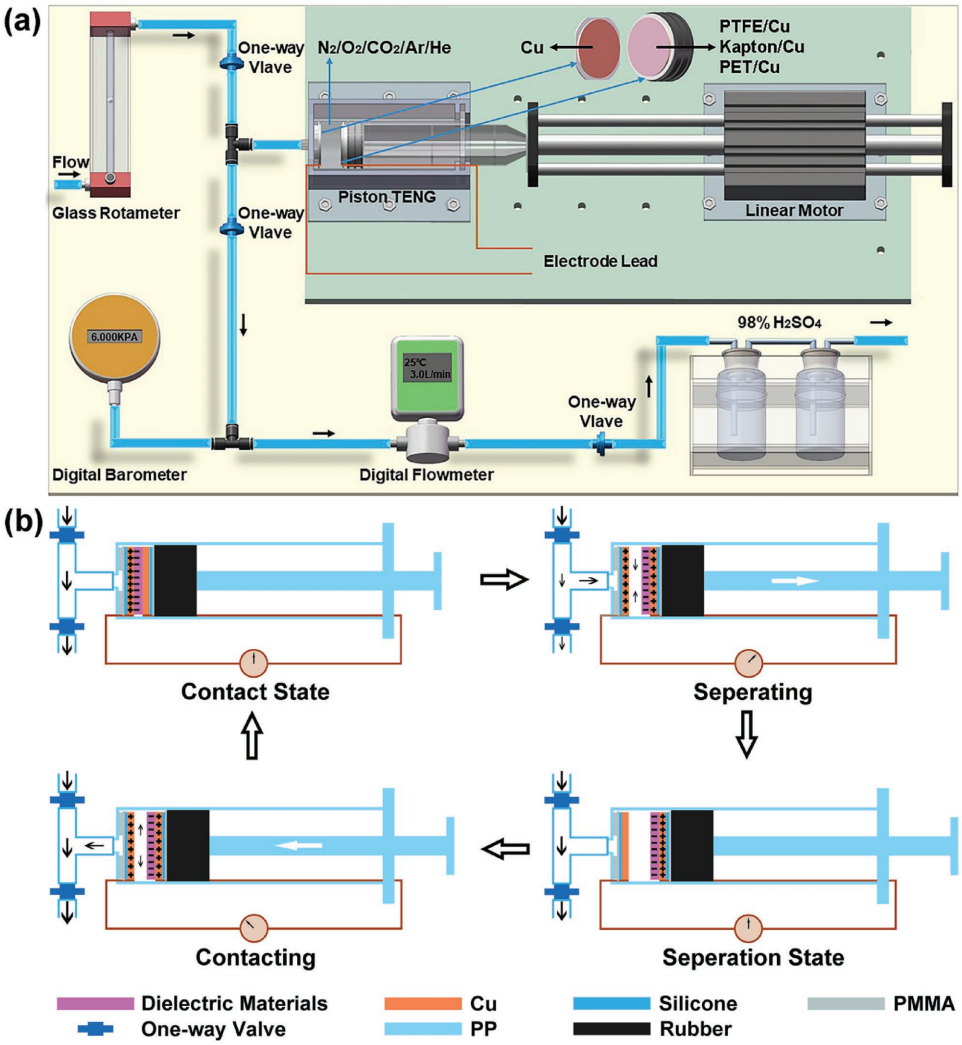

Figure 1. Experimental setup and working principle of piston TENG. a) Schematic diagram of experimental setup. b) Schematic working principle of piston TENG.

motor with predefined period setting (see the Experimental Section). Three different dielectric materials films (PTFE, Kapton, PET) and Cu film were selected to fabricate TENGs (see the Experimental Section). The circular Cu electrode with a radius of 2 cm was held in syringe barrel, and the polymer and its electrode with the same size were fixed on the other side. Then, pure gases (N_2, O_2, CO_2, Ar, He) flowed into the system, respectively. Figure 1b shows the working principle of the piston-structured TENG. After cycles of reciprocating motion, when the piston moves backward, a much higher potential on the Cu film side, which is attributed to the electric field generated by the separated surface charges, will drive the flow of positive charges to the other side through the external load. And when the piston moves forward to a close contact, an inverse positive potential built by the redistributed charges will drive transferred charges to flow back to Cu film side.[32] Meanwhile, the whole cycle is accompanied by gas coming in and out. Considering that the surface charge density determines the main basic performance of TENG,[31] two related performance indicators, Q_{SC} and open-circuit voltage (V_{OC}), are chosen to be measured directly by electrometer with a matched LabVIEW program on PC.

Since the test system is semiclosed, flow rate was chosen as the conference quantity first. In order to ensure enough gas supply and reduce potential damage to the system, flow rate was set at 3 L min^{-1}. Before each test, gas flux was set at the rate of 2 L min^{-1} for at least half an hour to remove the last remaining gas molecules and potential impurities as much as possible. When the flow rate was adjusted back, the linear motor was activated. After contact and separation proceeded repeatedly, the electrostatic charge on the surface would reach a saturation,[1] and then measurements of Q_{SC} and V_{OC} officially started. Statistical Q_{SC} data (**Figure 2**a–c) show that all three TENGs (PTFE-based, Kapton-based, PET-based) perform the best in CO_2, reaching to 40.29, 32.56, and 43.46 nC, respectively, while the worst in He, at 39.11, 17.47, and 33.46 nC correspondingly. With regard to other gases, the trend is that Q_{SC} value in O_2 is always bigger than in N_2. However, as for the atmosphere of Ar, Q_{SC} data demonstrate different results to Kapton-based TENG compared with two other TENGs. Meanwhile, multicycle

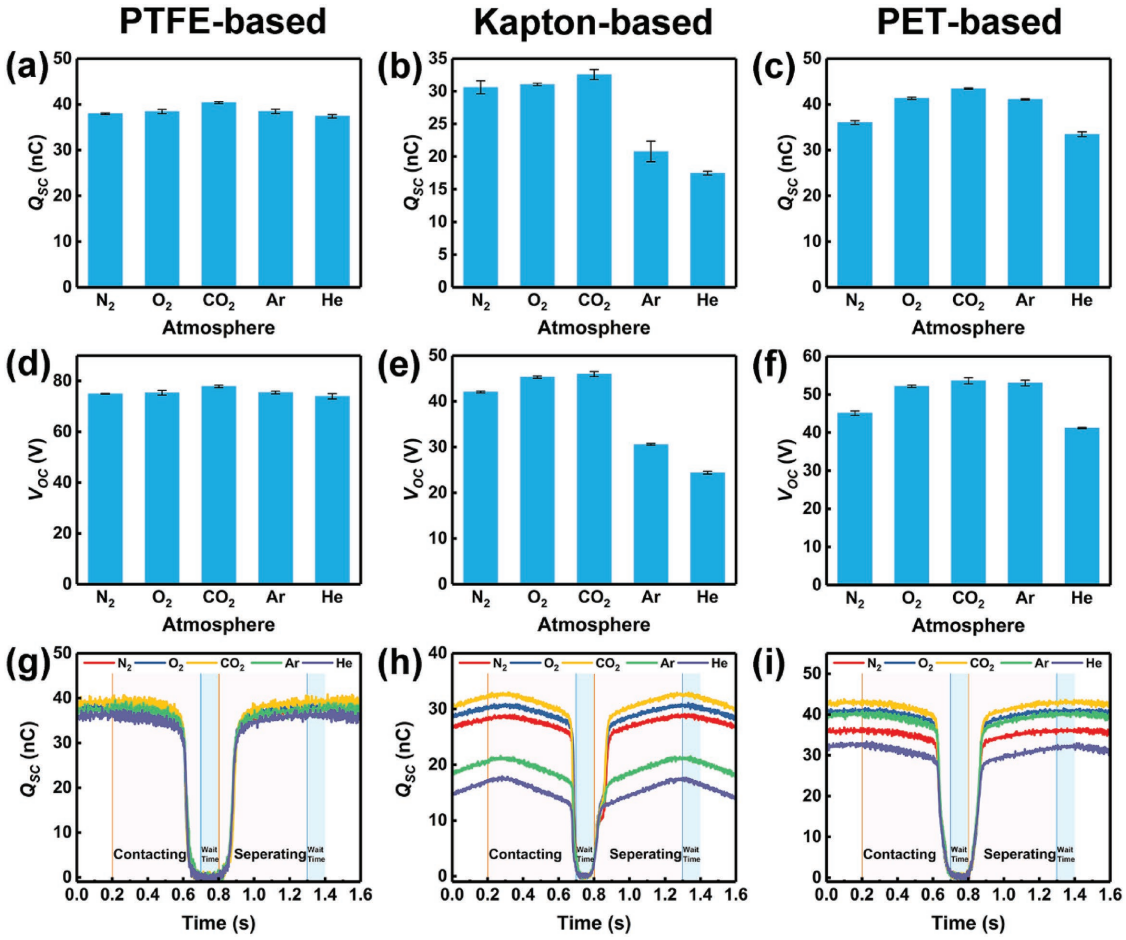

Figure 2. Multicycle statistical and single cycle performances of TENGs in different atmosphere at glass rotameter static gas flow rate of 3 L min^{-1}. a) Multicycle statistical Q_{SC} of PTFE-based TENG. b) Multicycle statistical Q_{SC} of Kapton-based TENG. c) Multicycle statistical Q_{SC} of PET-based TENG. d) Multicycle statistical V_{OC} of PTFE-based TENG. e) Multicycle statistical V_{OC} of Kapton-based TENG. f) Multicycle statistical V_{OC} of PET-based TENG. g) Single cycle Q_{SC} of PTFE-based TENG. h) Single cycle Q_{SC} of Kapton-based TENG. i) Single cycle Q_{SC} of PET-based TENG.

statistical V_{OC} in Figure 2d–f also shows similar trends with maximum values in CO_2 and minimum values in He, and different behavior in Ar to Kapton-based TENG. It is interesting to note that three TENGs have various disparities in different atmosphere, Kapton-based TENG shows the greatest, followed by PET-based TENG, and PTFE-based TENG. Taking the difference between in CO_2 and in He, for example, values are 2 nC of PTFE-based, 15 nC of Kapton-based and 10 nC of PET-based in turn. Such disparities are demonstrated more visually from the single cycle Q_{SC} data contrast in Figure 2g–i. The single-cycle proceeding time is represented by different background color, of which orange and dark blue lines mean acceleration and deceleration time respectively (around negligible 0.002 s), pink region for contacting and separating processes and light blue region for wait time. When at wait time of contact state, it is easy to find that the platform breadths of peak signals (shifted to zero position of vertical axis) are different. However, such difference may mainly due to the position error during different piston installation. And it has no regular relation with performance disparities as shown in later data. Besides, it is also worth noting that the Q_{SC} and V_{OC} values of different TENGs in one atmosphere has not performed as the same sequence of electron gain and loss among dielectric materials.[33,34] Nevertheless, this discrepancy is not contradictory, because they are totally two different concepts, one for absolute quantity and one for relative quantity. And the strength of the electron gain or loss can be simply verified by a TENG fabricated using two different dielectric materials.

To ensure the reliability of trends above, the reading of digital flowmeter was also used as a conference, adjusted at the rate of 3 L min^{-1} in the same way. The multicycle statistical Q_{SC} and V_{OC} data in Figure S1a–f of the Supporting Information similarly show the highest performance in CO_2 and the lowest in He. Other trends such like disparities and value orders in other gases are almost the same as that of using glass rotameter monitoring (Figure S1g–i, Supporting Information). Moreover, for the purpose of avoiding uncertain factors caused by long-time running, tests at the uniform condition but employing reverse gas replace order are conducted (Figure S2, Supporting Information). The results manifest that the gas test order has some influence in the value differences. However, the main trends that maximum and minimum values exist in which atmosphere condition and the disparity ranking has no change. Therefore, all of the data above indicate that different environmental atmosphere does

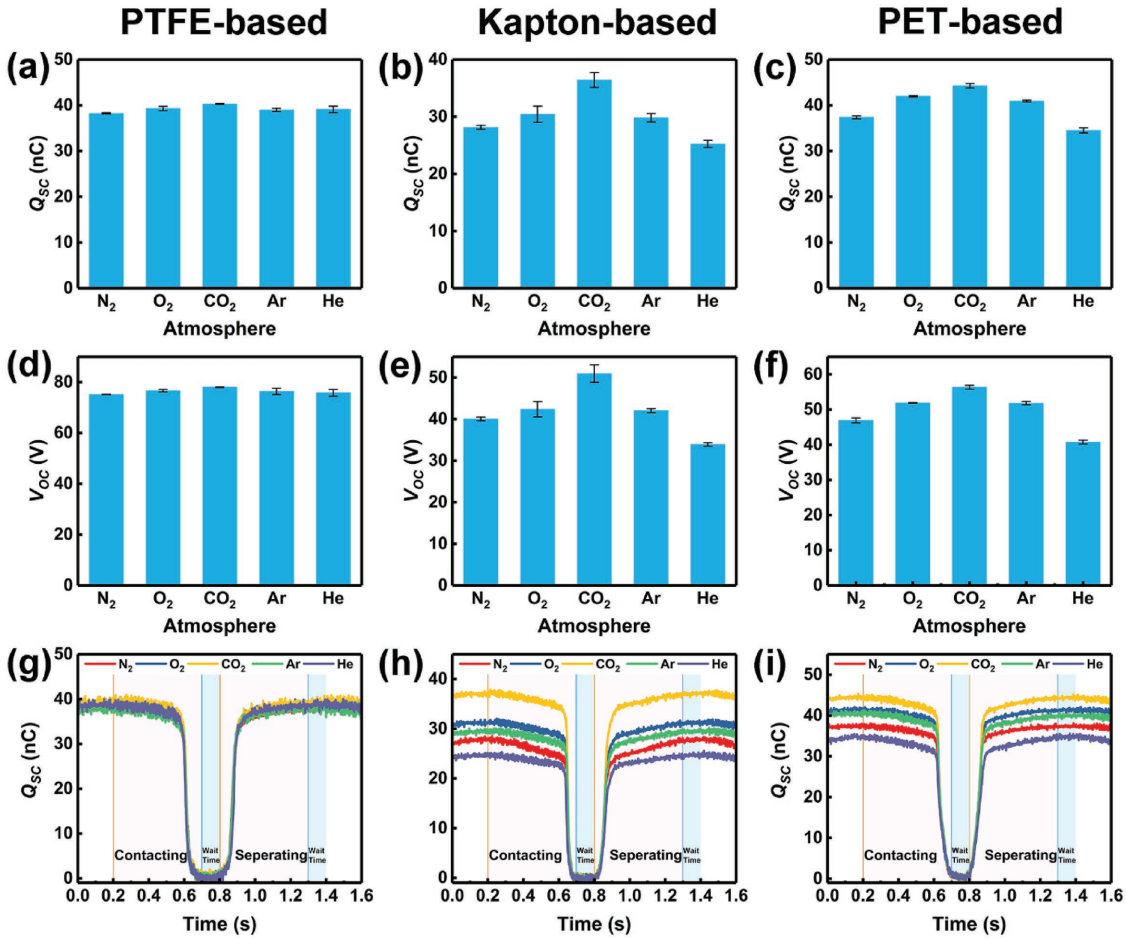

Figure 3. Multicycle statistical and single cycle performances of TENGs in different atmosphere at digital pressure gauge static gas pressure of 6 kPa above 1 atm. a) Multicycle statistical Q_{SC} of PTFE-based TENG. b) Multicycle statistical Q_{SC} of Kapton-based TENG. c) Multicycle statistical Q_{SC} of PET-based TENG. d) Multicycle statistical V_{OC} of PTFE-based TENG. e) Multicycle statistical V_{OC} of Kapton-based TENG. f) Multicycle statistical V_{OC} of PET-based TENG. g) Single cycle Q_{SC} of PTFE-based TENG. h) Single cycle Q_{SC} of Kapton-based TENG. i) Single cycle Q_{SC} of PET-based TENG.

have some impacts on the performance of TENG. And it is well worth doing further study to find more.

In another view, the same flow rate does not mean the same corresponding gas pressure (Table S1, Supporting Information), which will induce different resistance inevitably and may affect the acting force. Since the acting force plays an important role in the performance of TENG,[14,15] gas pressure as conference should be considered to eliminate the potential influence. By adjusting the gas input and using the digital pressure gauge, static gas pressure of 6 kPa above 1 atm (around 3 L min^{-1}) was set as new reference. As shown in **Figure 3**a–f, in spite of a much weaker statistical difference advantage for PTFE-based TENG, the performances in CO_2 are still the best in all three TENGs. Meanwhile, the minimum value of PTFE-based TENG changes from in He to in N_2. However, value in He has a larger error bar with lower limit less than in N_2, which means such change may be attributed to test error. And another two TENGs still show the same minimum value trend as before. In addition, the disparity distribution can be easily found in Figure 3g–i, especially PTFE-based TENG, with five single cycle data curves almost overlapped. It is important to note that the performance in O_2 is always better than in N_2, but the value in Ar plays an erratic role in the trend position all the time. In order to make the effects of different atmosphere more clearly, Kapton-based TENG, as always had the biggest disparity in various atmosphere, was employed to conduct an experiment with gas switching directly (Figures S3–S5, Supporting Information). Two pipelines were both set at the static pressure of 6 kPa above 1 atm in advance. When the Q_{SC} value reached a relative steady state, then switched to another gas promptly. Figure S3 of the Supporting Information indicates that when N_2, O_2, CO_2, and Ar were changed to He, respectively, the Q_{SC} value grew smaller quickly, and when switched back, the value recovered slowly. The same trend can be found in Figure S4 of the Supporting Information while switching to Ar directly. When N_2, O_2, and CO_2 are switched to each other (Figure S5, Supporting Information), it is observed that values in O_2 and CO_2 are both better than in N_2. But for the result between O_2 and CO_2, it does not show a uniform trend. Since it is hard to carry effective statistics for verifying the steady state, such trends above are for reference purpose only.

Besides, another parallel experiment was run at the static gas pressure of 3 kPa above 1 atm, results from Figure S6a,b of the Supporting Information demonstrate something interesting

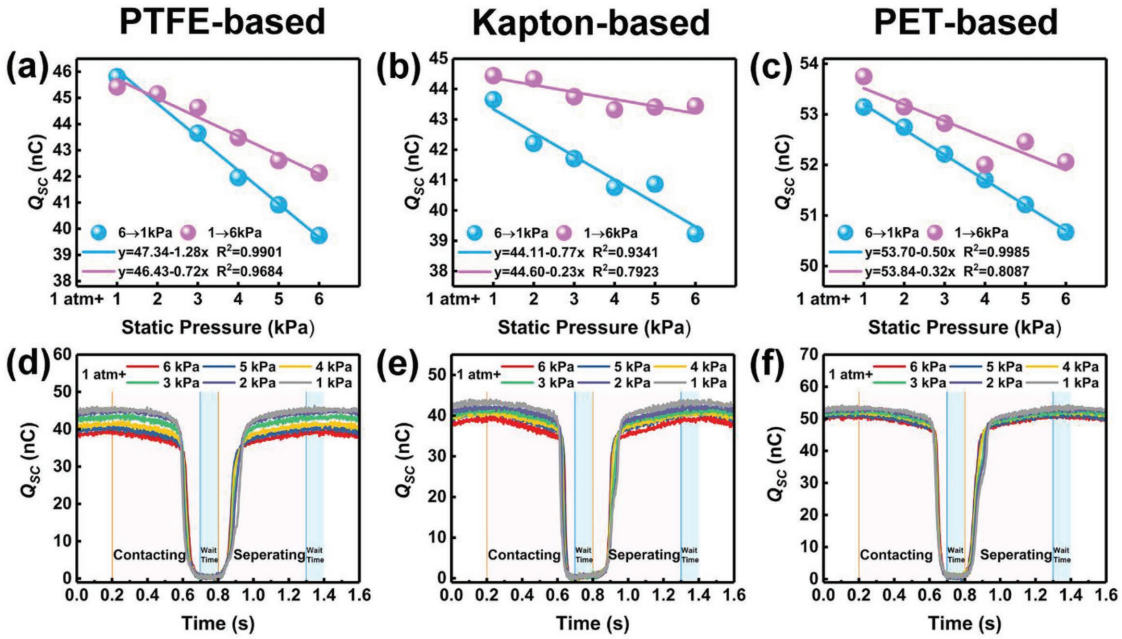

Figure 4. Multicycle statistical and single cycle performances of TENGs at different digital pressure gauge static N_2 pressure. a) Multicycle statistical Q_{SC} of PTFE-based TENG. b) Multicycle statistical Q_{SC} of Kapton-based TENG. c) Multicycle statistical Q_{SC} of PET-based TENG. d) Single cycle Q_{SC} of PTFE-based TENG. e) Single cycle Q_{SC} of Kapton-based TENG. f) Single cycle Q_{SC} of PET-based TENG.

that for PTFE-based TENG, the best average performance changes to in O_2 with a weak advantage of 0.55 nC. And for Kapton-based TENG, although the error bar upper limit in CO_2 is still a bit larger, the same matter comes. Based on the above discovery, it is inferred that gas pressure has some influence on the performance, and the type of dielectric materials also plays a significant role. The influence details need do further study as the disparities are still exists at the same reference pressure.

In order to investigate the specific effects of gas pressure, a series of tests on charge transfer were taken under different N_2 static pressure from 6 to 1 kPa above 1 atm. As shown in **Figure 4**a–c, there are negative linear relationships between Q_{SC} and static pressure at the given conditions with different slopes. To verify the reliability, after changing the static pressure from large to small, a reverse condition order followed by. It is easy to find that the linear relationships remained exist but with less sharp slopes. It is inferred that more electrostatic charges are accumulated on the material surface at a lower pressure and hard to reach a charge balance state at next pressure condition in a short time, resulting in different slopes. Furthermore, the same experiments were also performed in other four atmospheres using the PET-based TENG (Figure S7, Supporting Information). All of the data indicate that the transfer charge becomes bigger as the static gas pressure changing lower, though the value change is small. It is also interesting to note that a different slope value change is shown in He, which may be ascribed to more surface charge loss in this atmosphere. By adjusting the knob to the marked positions, another more visible contrast test was conducted under the continuous measuring state with the pressure directly changed to another and back then. The differences can be easily distinguished in Figure S8a–e,f of the Supporting Information shows the smoothed trends, using a six points Adjacent-Averaging method.

Since charge density plays an important part in the basic performance of TENG, any factors like pressure, gas adsorption, piston speed, roughness, and so on,[22–28] which will affect the process of contact electrification may influence the final performance. We carefully controlled experimental conditions (see the Experimental Section). A microscale gas discharge mechanism referencing to the literature is introduced to explain what we have found.[35–45] In addition, it is worth noting that our experimental surface charge density is relatively low, the gas breakdown following Paschen's law should not happen accordingly.[29,46]

According to the microscale discharge mechanism, when the piston moves backward, the strong electric field comes into being instantaneously.[41,46] Thus, a small amount of electrostatic surface charge might be excited into free electrons in space by quantum tunneling (**Figure 5**a).[38,45] Additionally, they will be accelerated by the electrostatic field, and collide with gas molecules further. As a result, more electrons, positive ions, even metastable state particles were generated, and may induce more interactions (Figure S9, Supporting Information).[36,45,47–49] As for positive ions, they are driven to approach the dielectric material surface by the effect of electric field, which may induce secondary electron emission as described in Townsend discharge and ion-enhanced field emission (Figure 5b).[37,45,50] According to the literature, in a range of microscale gap, the latter contributes much more.[41–44] When positive gaseous ions approach the dielectric material, the potential barrier lowers and thins, thus making more electrons emission easier.[41] The whole process is called electron emission, which is supposed to happen in our experiment. Consequently, the surface charge density decreases and further affects the performance of TENG. It is worth pointing out that our test trends of Q_{SC} and V_{OC} is related to the electron yield for various atmosphere in Radmilović-Radjenović's work.[44]

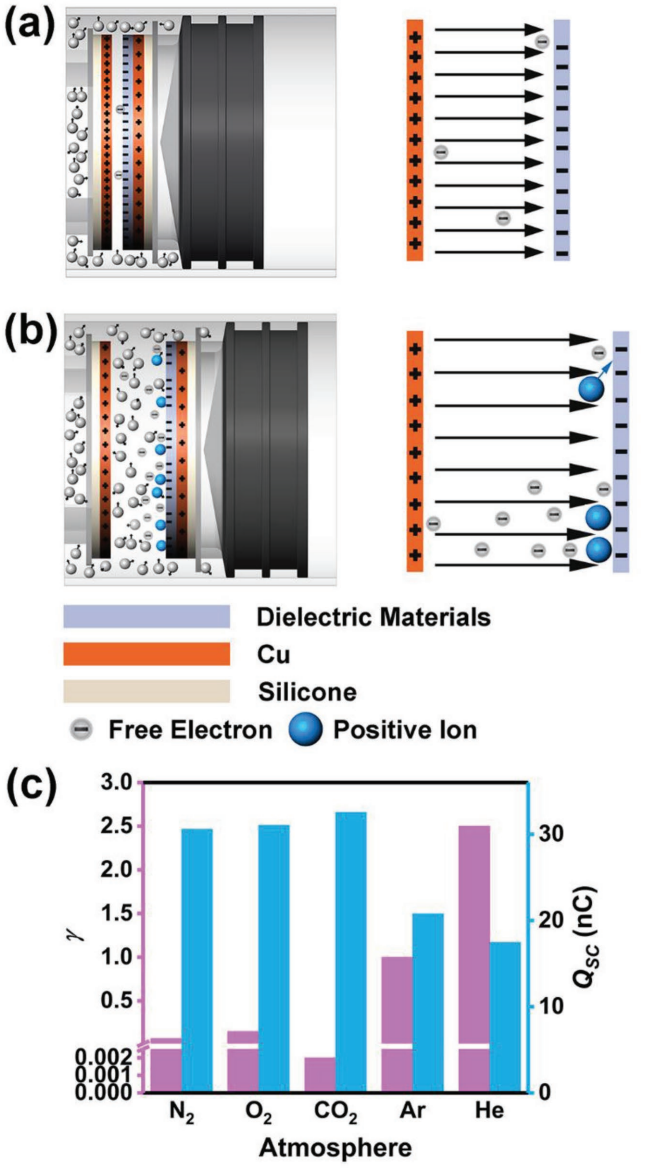

Figure 5. Schematic diagram of electron yield and comparison between γ and Q_{SC}. a) Process of electron emission by quantum tunneling. b) Process of electron emission by secondary electron emission and ion-enhanced field emission. c) Comparison between the value of the effective yield γ estimated from the line of dependence on the inverted electric field at 1.0 cm MV^{-1}[37] and Q_{SC} data from Kapton-based TENG at glass rotameter static gas flow rate of 3 L min^{-1}.

As shown in Figure 5c, it shows the comparison between the value of the effective yield γ estimated from the line of dependence on the inverted electric field at 1.0 cm MV^{-1} and Q_{SC} data from Kapton-based TENG.[44] It is observed that the less electrons yield the more Q_{SC} is got. In our system, low yields mean that more electrostatic charge could stay on the dielectric material surface and contribute to the TENG output. Moreover, in microscale gaps an explicit expression for electron yield per ion (γ) is also given from the literature as follows.[36,39,44]

$$\gamma = Ke^{-D/E} \quad (1)$$

where K and D are material and gas dependent constants, and E is the electric field in the gap. These dependency relationships can be good reference not only to explain well about the performance difference in different atmospheres but also to give a reason for the output disparity with different dielectric materials.

As for the effect of gas pressure in our test system, the output trend versus pressure is opposite from the reported work.[24,27] Therefore, it is speculated that higher pressure acting as a resistance causes less effective contact between materials and leads to lower initial charge density. As a result, the linear relationship between Q_{SC} and static gas pressure is negative.

3. Conclusion

In conclusion, a test system with controllable gas flow rate and pressure was constructed to investigate the effects of environmental atmosphere on the performance of TENG. By dint of one-way valves and piston-structured TENGs with different dielectric materials (PTFE, Kapton, PET) in contact–separation mode, five pure gases (N_2, O_2, CO_2, Ar, and He) were flowed into the system respectively to run series of Q_{SC} and V_{OC} measurements. At the same static gas flow rate or static gas pressure, multicycle statistics showed that TENGs performed almost the maximum in CO_2, and the minimum in He. Besides, Kapton-based TENG demonstrated the greatest performance disparity, followed by PET-based and PTFE-based. Moreover, it was found that Q_{SC} has a close minor negative linear relationship with static gas pressure in some range.

A microscale discharge mechanism was introduced to explain the performance difference in various atmospheres and the output disparity by using different dielectric materials. The electrons yielded by electron emission at microscale gaps, especially the ion-enhanced field emission, may have an important influence on the charge density and further affect the performance of TENG. Hence, this work will be an important reference to high-performance TENG and device packaging.

4. Experimental Section

Fabrication of Piston TENG: Three kinds of polymer tapes, PTFE (80 µm), Kapton (55 µm), and PET (50 µm) were selected as dielectric materials, and Cu tape (60 µm) was used as electrode material. Figure S10 of the Supporting Information shows the SEM images of three dielectric materials. All the surfaces are relatively smooth. Cu and dielectric material/Cu electrodes with radius of 2 cm were successively tacked to circular silicone pads and PMMA substrates, respectively. And the substrate containing only Cu electrode was designed with three holes to let gas flow in and out. Next, these two parts with conduct leads were fixed in the barrel and on the piston by double faced adhesive tape and AB epoxy glue separately. Then the piston TENG with sealing check was placed in a hand-made PMMA framework structure and fully fixed.

Fabrication of One-Way Valve Gas Line System: All gases (N_2, O_2, CO_2, Ar, and He) with purity of 99.999% were purchased from Praxair Technology, Inc. and delivered by food-grade silicone tube. The glass rotameter with knob (LZB-4WB, Xiang Yun Ltd.) was connected to the gas source, followed by two one-way valves in gas line with

a branch connected to the syringe. Then a digital pressure gauge (JT-118, Jia Tai Ltd.) and a digital flowmeter with temperature sensor (MF5700-N-10, Stargo Ltd.) were connected into the system. At the end of gas line, another one-way valve and double gas collecting bottles with concentrated sulfuric acid were placed in sequence.

Measurement of Piston TENG: The end of piston was mechanically connected on the same axis with a computer programmed linear motor. The movement distance was set at 1 cm, the maximum speed was set at 0.02 m s^{-1} with acceleration and deceleration speed both at 10 m s^{-2}. The loading cycle was about 1.2 s, including a wait time of 100 ms set at the contact and separation state respectively to get adequate contact and reduce the long-time load of motor. In addition, no obvious influence induced by piston speed and acceleration speed is observed (Figure S11, Supporting Information). The fixed volume change (about 12 mL) of TENG during the whole motion was measured by a dewatering method. The gas temperature (25 ± 2 °C) was monitored by temperature sensor of digital flowmeter. The room temperature was monitored by Thermometer and Humidity Meter (DT-625, CEM). The outside surface temperature of the syringe was monitored by IR thermometer (830-T2, Testo). All the temperature data were counted by frequency counts method (Figure S12, Supporting Information). The electrode leads were connected to the system electrometer (6514, Keithley) with a matched LabVIEW program on PC. Q_{SC} and V_{OC} were directly measured by using the corresponding functions of electrometer. Before each measurement, gas was flowed into the system at the rate of 2 L min^{-1} for at least half an hour. For one kind material of TENG, the tests in five gases were conducted by using the same one TENG. Each statistical data included three parallel tests with at least 50 continuous cycles at different references. As for the tests of changing gas type directly, three T-cock with switches were used to predefine the same pressure and control the change procedures.

Supporting Information

Supporting Information is available from the Wiley Online Library or from the author.

Acknowledgements

K.H. and W.T. contributed equally to this work. Research was supported by the National Key R&D Project from Minister of Science and Technology (2016YFA0202704), Beijing Municipal Science & Technology Commission (Z171100000317001, Z171100002017017, and Y3993113DF), and the National Natural Science Foundation of China (Grant Nos. 51432005, 5151101243, and 51561145021).

Conflict of Interest

The authors declare no conflict of interest.

Keywords

environmental atmosphere, microscale discharge, performance, piston structure, triboelectric nanogenerator

Received: October 30, 2018
Revised: November 17, 2018
Published online:

[1] Z. L. Wang, *Mater. Today* **2017**, *20*, 74.
[2] Z. L. Wang, *ACS Nano* **2013**, *7*, 9533.
[3] Z. L. Wang, J. Chen, L. Lin, *Energy Environ. Sci.* **2015**, *8*, 2250.
[4] B. Chen, Y. Yang, Z. L. Wang, *Adv. Energy Mater.* **2018**, *8*, 1702649.
[5] Z. L. Wang, T. Jiang, L. Xu, *Nano Energy* **2017**, *39*, 9.
[6] F.-R. Fan, Z.-Q. Tian, Z. L. Wang, *Nano Energy* **2012**, *1*, 328.
[7] S. Niu, S. Wang, L. Lin, Y. Liu, Y. S. Zhou, Y. Hu, Z. L. Wang, *Nano Energy* **2015**, *14*, 161.
[8] S. Niu, Y. S. Zhou, S. Wang, Y. Liu, L. Lin, Y. Bandob, Z. L. Wang, *Nano Energy* **2014**, *8*, 150.
[9] G. Zhu, B. Peng, J. Chen, Q. Jing, Z. L. Wang, *Nano Energy* **2015**, *14*, 126.
[10] X. Du, Y. Liu, J. Wang, H. Niu, Z. Yuan, S. Zhao, X. Zhang, R. Cao, Y. Yin, N. Li, C. Zhang, Y. Xing, W. Xu, C. Li, *ACS Appl. Mater. Interfaces* **2018**, *10*, 25683.
[11] R. Wen, J. Guo, A. Yu, K. Zhang, J. Kou, Y. Zhu, Y. Zhang, B.-W. Li, J. Zhai, *Nano Energy* **2018**, *50*, 140.
[12] V. Nguyen, R. Yang, *Nano Energy* **2013**, *2*, 604.
[13] H. Zhang, Y. Yang, Y. Su, J. Chen, Ch. Hu, Z. Wu, Y. Liu, C. P. Wong, Y. Bando, Z. L. Wang, *Nano Energy* **2013**, *2*, 693.
[14] J. Chen, P. Ding, R. Pan, W. Xuan, D. Guo, Z. Ye, W. Yin, H. Jin, X. Wang, S. Dong, J. Luo, *Nano Energy* **2017**, *34*, 442.
[15] H. Zhang, Y. Lu, A. Ghaffarinejad, P. Basset, *Nano Energy* **2018**, *51*, 10.
[16] J. Luo, F. R. Fan, T. Zhou, W. Tang, F. Xue, Z. L. Wang, *Extreme Mech. Lett.* **2015**, *2*, 28.
[17] Y. Zhu, B. Yang, J. Liu, X. Wang, L. Wang, X. Chen, C. Yang, *Sci. Rep.* **2016**, *6*, 22233.
[18] X.-S. Zhang, M.-D. Han, R.-X. Wang, B. Meng, F.-Y. Zhu, X.-M. Sun, W. Hu, W. Wang, Z.-H. Li, H.-X. Zhang, *Nano Energy* **2014**, *4*, 123.
[19] S. Wang, Y. Zi, Y. S. Zhou, S. Li, F. Fan, L. Lin, Z. L. Wang, *J. Mater. Chem. A* **2016**, *4*, 3728.
[20] S. Niu, Y. Liu, Y. S. Zhou, S. Wang, L. Lin, Z. L. Wang, *IEEE Trans. Electron Devices* **2015**, *62*, 641.
[21] X. Wen, Y. Su, Y. Yang, H. Zhang, Z. L. Wang, *Nano Energy* **2014**, *4*, 150.
[22] D. E. Debeau, *Phys. Rev.* **1944**, *66*, 9.
[23] F. R. Ruckdeschel, L. P. Hunter, *J. Appl. Phys.* **1975**, *46*, 4416.
[24] R. Elsdon, F. R. G. Mitchell, *J. Phys. D: Appl. Phys.* **1976**, *9*, 1445.
[25] J. Lowell, *J. Phys. D: Appl. Phys.* **1979**, *12*, 1541.
[26] B. A. Kwetkust, K. Sattler, H.-C. Siegmann, *J. Phys. D: Appl. Phys.* **1992**, *25*, 139.
[27] M. D. Hogue, C. R. Buhler, C. I. Calle, T. Matsuyama, W. Luo, E. E. Groop, *J. Electrost.* **2004**, *61*, 259.
[28] J. Lowell, A. C. Rose-Innes, *Adv. Phys.* **1980**, *29*, 947.
[29] J. Wang, C. Wu, Y. Dai, Z. Zhao, A. Wang, T. Zhang, Z. L. Wang, *Nat. Commun.* **2017**, *8*, 88.
[30] J. Chen, W. Tang, C. Lu, L. Xu, Z. Yang, B. Chen, T. Jiang, Z. L. Wang, *Appl. Phys. Lett.* **2017**, *110*, 201603.
[31] S. Niu, S. Wang, L. Lin, Y. Liu, Y. S. Zhou, Y. Hu, Z. L. Wang, *Energy Environ. Sci.* **2013**, *6*, 3576.
[32] S. Wang, L. Lin, Z. L. Wang, *Nano Lett.* **2012**, *12*, 6339.
[33] L. S. McCarty, G. M. Whitesides, *Angew. Chem., Int. Ed.* **2008**, *47*, 2188.
[34] Z. L. Wang, L. Lin, J. Chen, S. Niu, Y. Zi, *Triboelectric Nanogenerators*, Springer, Switzerland **2016**.
[35] F. L. Jones, *Nature* **1952**, *170*, 601.
[36] W. S. Boyle, P. Kisliuk, *Phys. Rev.* **1955**, *97*, 255.
[37] T. Ono, D. Y. Sim, M. Esashi, *J. Micromech. Microeng.* **2000**, *10*, 445.
[38] A. Wallash, L. Levit, *Proc. SPIE* **2003**, *4980*, 87.
[39] M. Radmilović-Radjenović, B. Radjenović, *Plasma Sources Sci. Technol.* **2008**, *17*, 024005.
[40] P. M. Ireland, *J. Electrost.* **2009**, *67*, 462.
[41] D. B. Go, D. A. Pohlman, *J. Appl. Phys.* **2010**, *107*, 103303.

[42] A. Venkattraman, A. A. Alexeenko, *Phys. Plasmas* **2012**, *19*, 123515.
[43] M. Radmilović-Radjenović, S. Matejčik, M. Klas, B. Radjenović, *J. Phys. D: Appl. Phys.* **2013**, *46*, 015302.
[44] M. Radmilović-Radjenović, B. Radjenović, S. Matejčik, M. Klas, *Plasma Chem. Plasma Process.* **2014**, *34*, 55.
[45] D. B. Go, A. Venkattraman, *J. Phys. D: Appl. Phys.* **2014**, *47*, 503001.
[46] Y. Zi, C. Wu, W. Ding, Z. L. Wang, *Adv. Funct. Mater.* **2017**, *27*, 1700049.
[47] N. Baguer, A. Bogaerts, Z. Donko, R. Gijbels, N. Sadeghi, *J. Appl. Phys.* **2005**, *97*, 123305.
[48] Y. Itikawa, *J. Phys. Chem. Ref. Data* **2002**, *31*, 749.
[49] H. Hotop, E. Kolb, J. Lorenzen, *J. Electron Spectrosc. Relat. Phenom.* **1979**, *16*, 213.
[50] Y. P. Raizer, *Gas Discharge Physics*, Springer, Berlin **1991**.